Microsc. Microanal. 19, S5, 77–82, 2013
doi:10.1017/S1431927613012385

Scale-Bridging Analysis on Deformation Behavior of High-Nitrogen Austenitic Steels

Tae-Ho Lee,[1,*] Heon-Young Ha,[1] Byoungchul Hwang,[2] Sung-Joon Kim,[3] Eunjoo Shin,[4] and Jong Wook Lee[5]

[1]*Ferrous Alloy Department, Advanced Metallic Materials Division, Korea Institute of Materials Science, 797 Changwondaero, Changwon 642-831, South Korea*
[2]*Department of Materials Science & Engineering, Seoul National University of Science and Technology, 232 Gongneung, Nowon, Seoul 139-743, South Korea*
[3]*Graduate Institute of Ferrous Technology, Pohang University of Science & Technology, San 31 Hyoja, Nam, Pohang 790-784, South Korea*
[4]*Neutron Physics Department, Korea Atomic Energy Research Institute, P.O.B. 105, Yuseong, Daejeon 305-600, South Korea*
[5]*Doosan Heavy Industries & Construction, Changwon 642-792, South Korea*

Abstract: Scale-bridging analysis on deformation behavior of high-nitrogen austenitic Fe–18Cr–10Mn–(0.39 and 0.69)N steels was performed by neutron diffraction, electron backscattered diffraction (EBSD), and transmission electron microscopy (TEM). Two important modes of deformation were identified depending on the nitrogen content: deformation twinning in the 0.69 N alloy and strain-induced martensitic transformation in the 0.39 N alloy. The phase fraction and deformation faulting probabilities were evaluated based on analyses of peak shift and asymmetry of neutron diffraction profiles. Semi *in situ* EBSD measurement was performed to investigate the orientation dependence of deformation microstructure and it showed that the variants of ε martensite as well as twin showed strong orientation dependence with respect to tensile axis. TEM observation showed that deformation twin with a $\{111\}\langle 11\bar{2}\rangle$ crystallographic component was predominant in the 0.69 N alloy whereas two types of strain-induced martensites (ε and α' martensites) were observed in the 0.39 N alloy. It can be concluded that scale-bridging analysis using neutron diffraction, EBSD, and TEM can yield a comprehensive understanding of the deformation mechanism of nitrogen-alloyed austenitic steels.

Key words: scale-bridging analysis, deformation, high-nitrogen austenitic steels, neutron diffraction, EBSD, TEM

Introduction

It is important to understand the fundamental aspects of material properties based on microstructure analyses using various experimental techniques including electron microscopy and X-ray or neutron diffraction. When the deformation mechanism of austenitic steels is taken into account, most investigations, so far, have used a specific experimental technique, and thereby the scale covered by the analysis has been limited. The dislocation configuration and crystallography of deformation products (deformation faults, strain-induced martensites) have well been characterized by transmission electron microscopy (TEM), and some attempts to understand the deformation mechanism have been made (Venables, 1962; Fujita & Mori, 1972; Idrissi et al., 2007; Lee et al., 2007). However, TEM investigation has an inherent shortcoming due to its narrow sampling area, and thus the statistical problems should be overcome. Although X-ray or neutron diffraction can provide a much wider range of information, it is difficult to obtain the submicron-scale information on deformation microstructure. This is why the scale-bridging analysis is required to gain comprehensive understanding of the deformation mechanism.

*Corresponding author. E-mail: lth@kims.re.kr

In austenitic steels, considerable efforts and discussions have been directed toward understanding two important modes of deformation, strain-induced martensitic transformation (SIMT) and deformation twinning (DT), owing to their favorable contribution to the considerable enhancement of steel properties. Therefore, they have remained a subject of practical importance in the development of high-performance austenitic steels (Remy & Pineau, 1977; Lee et al., 2008), and the control of deformation mode can provide a foundation in expanding the application field of austenitic steels.

The present paper aimed to provide an understanding of deformation behavior of austenitic Fe–18Cr–10Mn–N alloys. To understand the nitrogen-induced change in deformation mode from SIMT to DT, scale-bridging analysis using neutron diffraction, electron backscattered diffraction (EBSD), and scanning transmission electron microscopy (STEM) was performed as shown in Figure 1.

Materials and Methods

Materials

Two austenitic stainless steels with a base composition of Fe–18Cr–10Mn containing 0.39 and 0.69 N (all are in wt%) were fabricated utilizing a pressurized induction melting

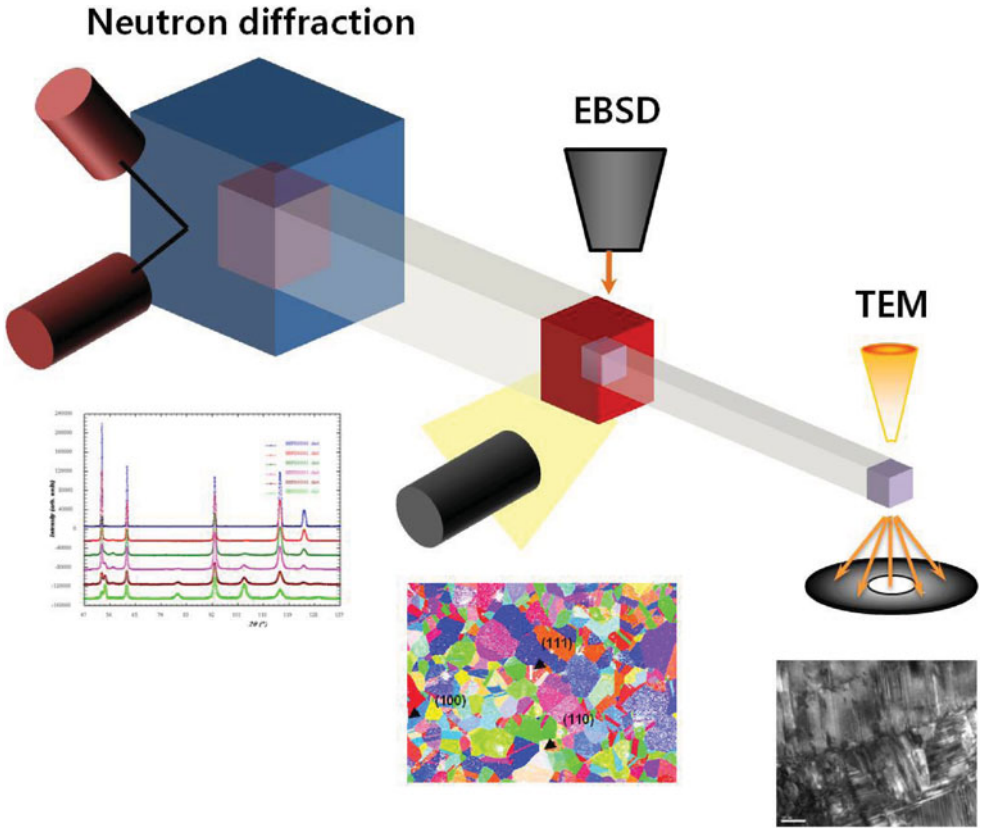

Figure 1. Schematic illustration of the concept of scale-bridging analysis. EBSD, electron backscattered diffraction; TEM, transmission electron microscopy.

furnace (VIM 4 III-P, ALD, Germany) under nitrogen gas pressures of 1 and 5 bar. After homogenization at 1,200°C for 2 h under an argon atmosphere, the ingots were hot-rolled into sheets of 4 mm thickness, followed by air cooling. The specimens were solution annealed at temperatures of 1,050 and 1,100°C for 1 h and then quenched into water. Five specimens (ASTM E8M) for each alloy were tensile-tested at room temperature at a nominal strain rate of 1.67×10^{-3}/s using a servohydraulic machine (Instron 5882, Canton, MA, USA).

Neutron Diffraction

Neutron diffraction experiments were conducted using a high-resolution powder diffractometer equipped with 32 detectors at HANARO, Korea Atomic Energy Research Institute, South Korea. The neutron beam was monochromatized to a wavelength of 1.8344 Å, and its spatial extension at the specimen level was 30 × 60 mm. The data were collected at intervals of 0.05° between 30 and 140° in the 2θ range (Lee et al., 2006). In whole-profile fitting using a modified Thompson–Cox–Hasting pseudo-Voigt function (Thompson et al., 1987), a total of 16 parameters were refined using a FullProf program (Rodriguez-Carvajal, 1998).

Microstructural Observation

To investigate the change in crystallographic orientation, the specimen was uniaxially elongated using a semi *in situ* deformation stage incorporated into a field emission gun scanning electron microscope (JSM 6500F, JEOL, Japan). The characteristics of orientation rotation were analyzed using an EBSD system (Inca Crystal). A detailed description on semi *in situ* EBSD and TEM observation has been provided in our previous paper (Lee et al., 2007).

Results and Discussion

Transition of Deformation Mode

When the Fe–18Cr–10Mn–(0.39 and 0.69)N alloys were subjected to tensile loading, deformation mode was changed from SIMT to DT with increasing nitrogen content. The σ–ε curves of the alloys are shown in Figure 2 together with incremental work-hardening exponents. The effects of nitrogen on stress–strain response can be manifested by the changes in the shape of the σ–ε curve (solid lines) and work-hardening exponents (symbols). In the 0.69 N alloy, the flow stress increased monotonously with increasing strain up to fracture, whereas the shape of the σ–ε curve of the 0.39 N alloy transformed into a sigmoidal form at a transient strain (Lee et al., 2008). The change in incremental work-hardening exponents also showed a sigmoidal shape, from which the occurrence of SIMT could be distinguished more clearly. The uniform elongations, obtained from the intercept of $\varepsilon = n_{inc}$ (dotted lines), were 0.382 and 0.504 in 0.69 N and 0.39 N alloys, respectively. It can be deduced that the occurrence of SIMT considerably increased the work-hardening exponents as well as uniform elongation of

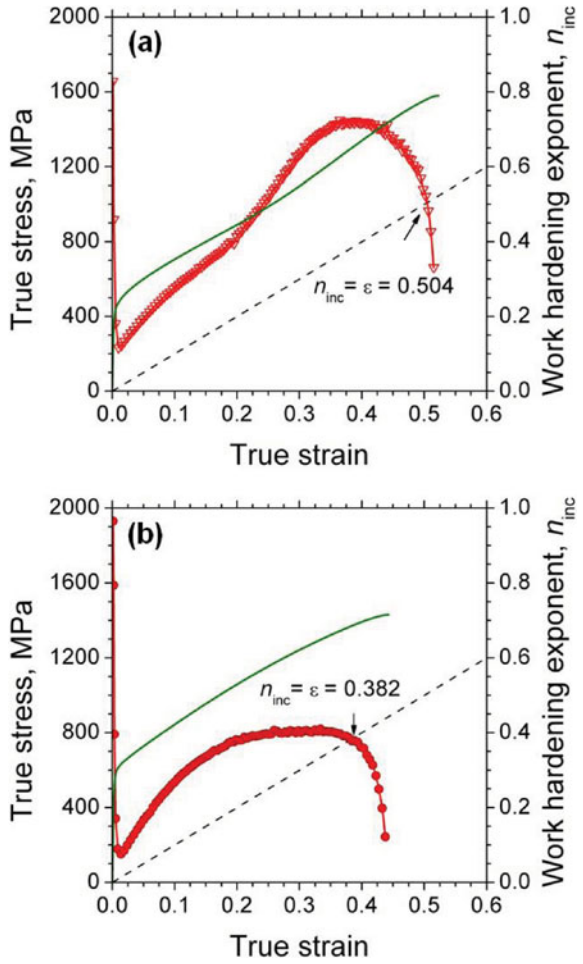

Figure 2. True stress–true strain curves and incremental work-hardening exponents of (**a**) 0.39 N and (**b**) 0.69 N alloy, respectively.

the 0.39 N alloy. The yield strength, on the other hand, increased almost linearly with increasing nitrogen contents.

Neutron Diffraction Analysis

Quantitative information on deformation microstructure of 0.39 N was obtained from the change in volume fractions of constituent phases (γ, ε, and α'), and the calculated results are summarized in Table 1. In the early stage of deformation, the ε martensite started to form and reached its maximum. Then, the volume fraction decreased upon further deformation. The α' martensite formed after a certain amount of strain ($\varepsilon = 0.2$), and further deformation led to a steady increase in its volume fraction. The decrease in the volume fraction of ε martensite at a higher strain region implies that the α' martensite formed at the expense of ε martensite and the nucleation site of α' martensite is closely related to the overlapping ε martensites.

Table 1. Quantitative Information on Deformation Microstructure Measured by Neutron Diffraction.

	0.39 N Phase Fraction (%)			0.69 N
	γ	ε	α'	TFP ($\times 10^3$)
0.1	97.96	2.21	0.74	1.02
0.2	83.63	10.87	5.50	1.80
0.3	79.59	8.89	11.51	3.12
0.4	56.13	7.56	36.81	4.36
0.5	41.24	6.92	51.84	—

TFP, twin fault probabilities.

For the 0.69 N alloy, whose main deformation mode is DT, a quantitative analysis of deformation microstructure can be carried out by the calculation of twin fault probabilities (TFP, β). According to the following equation proposed by Wagner (1966), the probability of finding DT can be calculated by measuring the difference between the position of the center of gravity and the peak maximum. The variations of TFP for the 0.69 N alloy as a function of true strain are shown in Table 1. At a low strain of $\varepsilon = 0.1$, the TFP was calculated to be 1.02×10^{-3} and increased steadily with the degree of tensile deformation. In a general trend, the TFP showed an almost linear relationship with increasing strain and reached its maximum value of 4.36×10^{-3} at $\varepsilon = 0.4$.

Orientation Dependence of Deformation Microstructure

Figure 3a shows the EBSD maps taken from the 0.39 N alloy showing the change in orientation before and after tensile deformation ($\varepsilon = 0.1$). The microstructure of the undeformed specimen is characterized by fully recrystallized grains with a random texture and Σ3-type annealing twins. As deformation proceeded, the crystal orientation rotated and the degree of rotation varied depending on their relative orientation with respect to tensile axis. In grains with ⟨001⟩ and ⟨111⟩ orientations, they retained their original orientation or rotated slightly along the [001]-[111] boundary line. On the other hand, the grains with other orientations, especially those with near ⟨110⟩ orientation, showed a significant degree of lattice rotation.

To investigate the corresponding deformation microstructure after semi *in situ* EBSD mapping, thin foils with ⟨110⟩, ⟨111⟩, and ⟨100⟩ orientations were prepared using focused ion beam. In the ⟨111⟩ grain (Fig. 3b), three ε variants were formed along $\langle 11\bar{2} \rangle$ directions of γ. The ε observed were crystallographically related to the γ in accordance with the Shoji–Nishiyama relation (Nishiyama, 1971), where the close-packed planes and directions are parallel. In the case of the ⟨110⟩ grain, only one ε variant could be identified in the initial stage of deformation, but further deformation activated other ε variants, resulting in their mutual intersection, as shown in Figure 3c. The deformation bands consisted of many overlapping ε (as shown in the magnified image), and they also showed the S–N orientation relationship (OR) with γ. In some regions wherein two ε intersected with each other, the α' formed and the OR between γ and α' was determined to be that of the Nishiyama–Wassermann (N–W) relation (Nishiyama, 1971). In contrast to the ⟨110⟩ and ⟨111⟩ orienta-

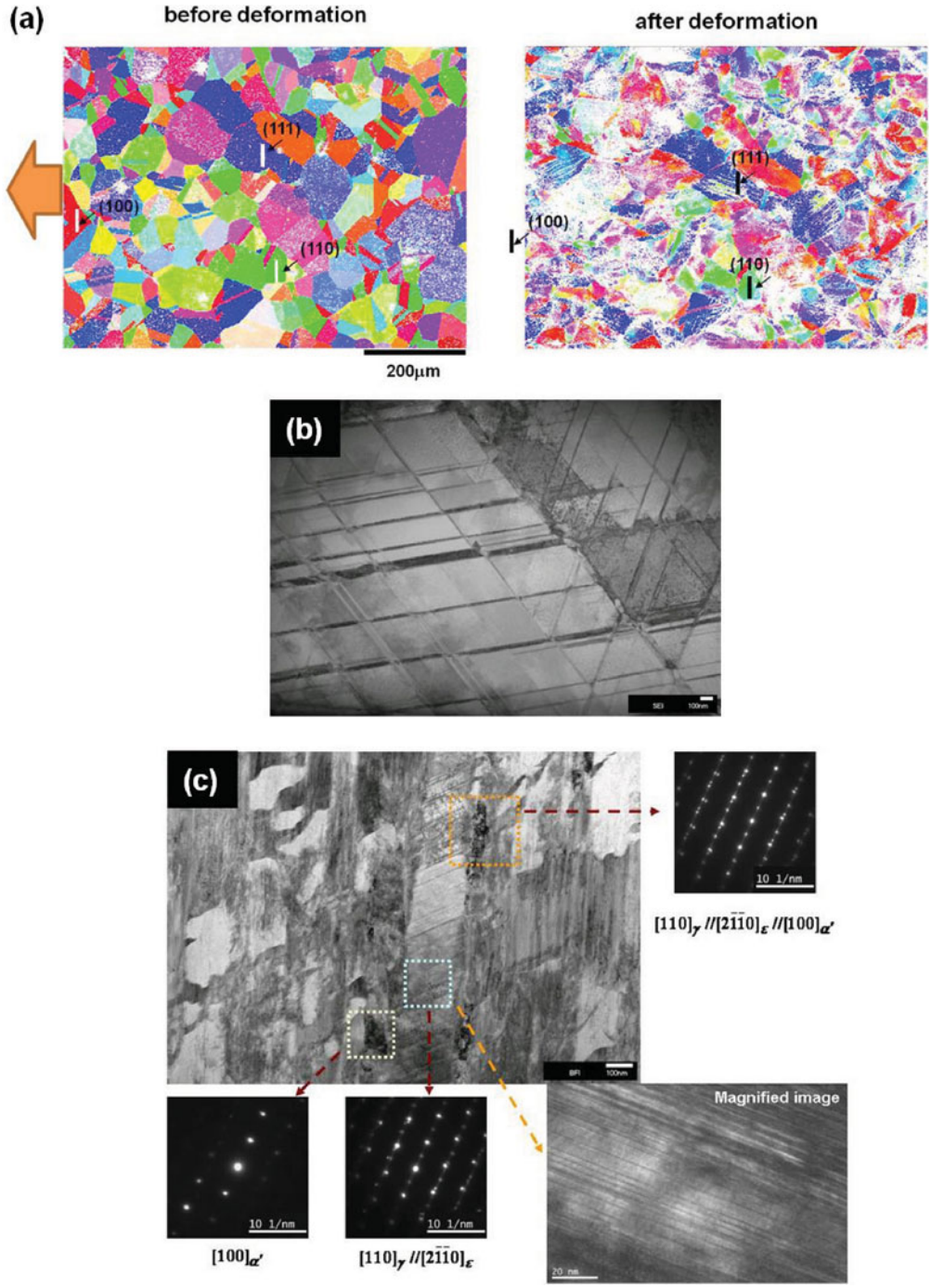

Figure 3. a: Electron backscattered diffraction maps showing the change in orientation before and after tensile deformation ($\varepsilon = 0.1$) taken from the 0.39 N alloy, (**b**) scanning transmission electron microscopy bright field (STEM BF) image of the ⟨111⟩ orientation ($\varepsilon = 0.2$) showing three variants of ε martensites, and (**c**) STEM BF image and corresponding SAD patterns taken from the ⟨110⟩ specimen ($\varepsilon = 0.3$), respectively.

tions, there was no ε martensite in the ⟨001⟩ orientation. A similar orientation dependence of DT with respect to tensile axis was also observed in our previous study (Lee et al., 2007).

TEM Observation on Deformation Microstructure

In the early stage of deformation, the glide of planar dislocations and formation of various types of stacking fault (SF) were identified, and the widths of SF were varied by a large extent. Upon further deformation, the SF tended to overlap or to extend along a preferential $\{111\}_\gamma$. As the tensile deformation proceeded, two types of strain-induced martensites were identified, as described in the previous section. Figures 4a–4c show the TEM bright field (BF) images of ε martensite, SAD pattern, and the calculated SAD pattern of the 0.39 N alloy strained to $\varepsilon = 0.2$. The ε formed at the

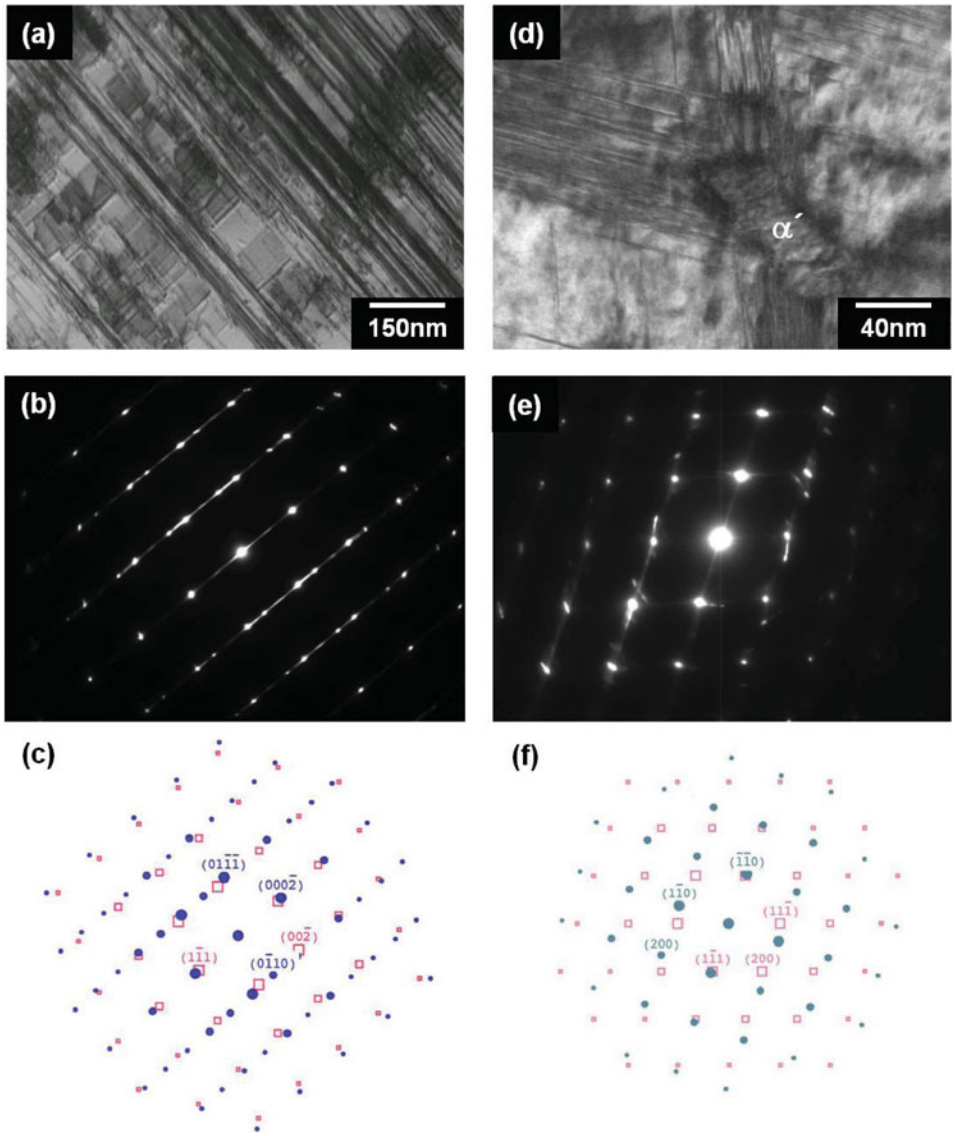

Figure 4. Transmission electron microscopy micrographs of ε ($\varepsilon = 0.2$) and α' martensite ($\varepsilon = 0.3$) taken from the 0.39 N alloy: (**a**) bright field (BF) image of ε martensite, (**b**) SAD pattern ($z = [110]_\gamma \| [\bar{2}110]_\varepsilon$), (**c**) calculated SAD pattern of (**b**) (open red squares, the γ matrix; blue-filled circles, the ε martensite), (**d**) BF image of α' martensite indicated by arrow, (**e**) SAD pattern showing Nishiyama–Wassermann orientation relationship ($z = [110]_\gamma \| [001]_{\alpha'}$), and (**f**) computer-simulated SAD pattern of (**b**) (open red squares, the γ matrix; green-filled circles, the α' martensite).

overlapped SF and grew with planar morphology along $\{111\}_\gamma$. The ε martensite observed had three variants of growth directions parallel to $\langle 11\bar{2}\rangle$ and the close-packed (0001) planes of ε martensite were aligned with the close-packed $\{111\}_\gamma$ (Nishiyama, 1971).

Figures 4d–4f show BF images showing the formation of α' martensite, SAD pattern, and the calculated SAD pattern for the 0.39 N alloy strained up to $\varepsilon = 0.3$. The α' martensite nucleated at the intersection of ε variants (Fig. 4d) and the characteristic streaks in the SAD pattern correspond to the parallel traces of ε (Fig. 4e). The OR relationship between γ and α' was determined from composite SAD patterns using known beam directions of γ and could be indexed either as an N–W or as a Kurdjumov–Sachs relation (Nishiyama, 1971). As an example, the OR corresponding to the N–W relation shown in Figure 4e can be expressed as $[110]_\gamma \| [001]_{\alpha'}$ and $(1\bar{1}1)_\gamma \| (110)_{\alpha'}$.

In the 0.69 N alloy, the planar dislocation arrays were dominant at the beginning of deformation, similar to the case of SIMT alloys. Further deformation showed particular features of microstructure, e.g., extended SF, dipolar dislocation groups, and dislocation pile-ups at grain boundaries. At higher strain, deformation microstructure mainly consisted of pronounced DT. The deformation bands formed in the 0.69 N alloy consist of nanosized twins lying along the $\langle 112\rangle$ direction. In general, the width of a twin band is not uniform, but varies slightly from one part of the band to another. Further deformation induced the activation of twin bands on another {111} slip plane and thereby the intersection between two or more twin bands became eas-

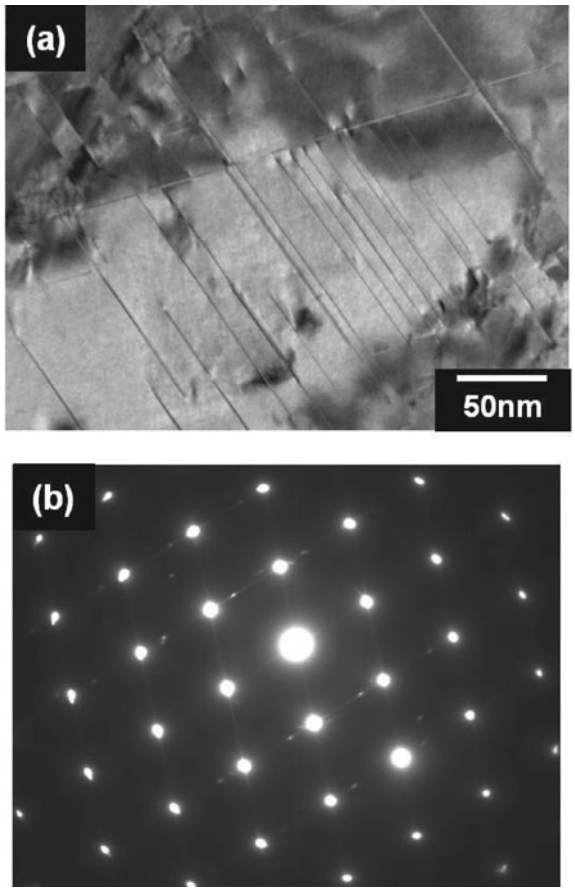

Figure 5. Transmission electron microscopy micrographs of deformation twinning taken from the 0.69 N alloy ($\varepsilon = 0.3$); (**a**) bright field image and (**b**) SAD pattern ($z = [110]_\gamma$) corresponding to the primary and conjugate twinning system.

ier. Figure 5 shows a typical BF image and SAD pattern taken from the 0.69 N alloy strained to $\varepsilon = 0.3$. At this deformation stage, the primary and the conjugate twinning system interacted, and each twinning component was distinguished in the SAD pattern where primary twinning manifested as diffraction spots.

Conclusions

Scale-bridging analysis on the deformation behavior of austenitic Fe–18Cr–10Mn– (0.39 and 0.69)N steels was performed by neutron diffraction, EBSD, and TEM, and the following conclusions can be drawn.

1. Two important modes of deformation were identified depending on the nitrogen content: DT in the 0.69 N alloy and SIMT in the 0.39 N alloy, respectively.
2. Based on the analysis of neutron diffraction profiles, the faulting probabilities as well as the volume fractions of strain-induced martensites were calculated.
3. Semi *in situ* tensile EBSD measurement revealed that the variants of ε martensite as well as twin showed strong orientation dependence with respect to tensile axis.
4. In SIMT alloys, the $\gamma \rightarrow \varepsilon \rightarrow \alpha'$ martensitic transformation sequentially occurred with increasing strain and the α' martensite contributed toward a good balance of tensile strength and uniform elongation. On the other hand, the deformation microstructure of the DT alloy mainly consisted of pronounced DT.

Acknowledgments

This work was financially supported by the Ministry of Knowledge Economy, Korea. The authors would like to express their gratitude to Mrs Jong-In Bae and Sung-Tae Kim for their valuable support in the experimental works.

References

Fujita, H. & Mori, T. (1972). Stacking faults and f.c.c. (γ) → h.c.p. (ε) transformation in 18/8-type stainless steel. *Acta Metall* **20**, 759–767.

Idrissi, H., Renard, K., Ryelandt, L., Schryvers, D. & Jacques, P.J. (2007). On the mechanism of twin formation in Fe-Mn-C TWIP steels. *Acta Mater* **58**, 2464–2476.

Lee, T.-H., Kim, S.-J., Shin, E. & Takaki, S. (2006). On the crystal structure of Cr_2N precipitates in high-nitrogen austenitic stainless steel (III) neutron diffraction study on the ordered Cr_2N superstructure. *Acta Cryst* **62**, 979–986.

Lee, T.-H., Oh, C.-S. & Kim, S.-J. (2008). Effects of nitrogen on deformation-induced martensitic transformation in metastable austenitic Fe-18Cr-10Mn-N steels. *Scripta Mater* **58**, 110–113.

Lee, T.-H., Oh, C.-S., Kim, S.-J. & Takaki, S. (2007). Deformation twinning in high nitrogen austenitic stainless steel. *Acta Mater* **55**, 3649–3662.

Nishiyama, Z. (1971). *Martensitic Transformation*. New York: Academic Press Inc.

Remy, L. & Pineau, A. (1977). Twinning and strain-induced f.c.c. → h.c.p. transformations in the Fe–Mn–Cr–C system. *Mater Sci Eng* **28**, 99–107.

Rodriguez-Carvajal, J. (1998). *FullProf, Version 3.5d*. Saclay, France: Laboratoire Leon Brillouin.

Thompson, P., Cox, D.E. & Hastings, J.B. (1987). Rietveld refinement of Debye-Scherrer synchrotron X-ray data from Al_2O_3. *J Appl Cryst* **20**, 79–83.

Venables, J.A. (1962). The martensite transformation in stainless steels. *Phil Mag* **7**, 35–44.

Wagner, C.N.J. (1966). Analysis of the broadening and change in position of peaks in an X-ray powder pattern. In *Local Atomic Arrangement Studied by X-Ray Diffraction*, Cohen, J.B. & Hilliard, J.E. (Eds.). pp. 219–269. New York: Gordon and Breach.